



# Enhanced mechanical and thermal properties of fly ash-based geopolymer composites by wollastonite reinforcement

Khanthima HEMRA<sup>1,2</sup>, Takaomi KOBAYASHI<sup>3</sup>, Pavadee AUNGKAVATTANA<sup>4</sup>, and Sirithan JIEMSIRILERS<sup>1,2,\*</sup>

<sup>1</sup> Department of Materials Science, Faculty of Science, Chulalongkorn University, Phayathai Rd., Pathumwan, Bangkok, 10330 Thailand

<sup>2</sup> Center of Excellence on Petrochemical and Materials Technology, Chulalongkorn University, Pathumwan, Bangkok 10330, Thailand.

<sup>3</sup> Department of Materials Science and Technology, Nagaoka University of Technology, 1603-1 Kamitomioka, Nagaoka, Niigata, 9402188 Japan

<sup>4</sup> National Nanotechnology Center, 111 Thailand Science Park, Paholyothin Rd., Klong Luang, Pathum thani, 12120 Thailand

\*Corresponding author e-mail: sirithan.j@chula.ac.th

## Received date:

3 August 2021

## Revised date

13 September 2021

## Accepted date:

19 October 2021

## Keywords:

Wollastonite;  
Geopolymer composite;  
Compressive strength;  
Thermal stability;  
Dilatometry

## Abstract

The present study investigated the mechanical and thermal properties of geopolymer composite. The geopolymer composite was prepared by mixing fly ash and wollastonite with the alkaline activator, which was 6 M KOH:K<sub>2</sub>SiO<sub>3</sub> in a mass ratio of 1:1 and a solid:liquid mass ratio of 3:2. The compressive strength at 28 days of geopolymer was 33.3 MPa and possessed the highest strength of 38.3 MPa when 30 wt% wollastonite was added. The flexural strength presented differently whereby it increased from 2.1 MPa to 6.8 MPa. It increased remarkably up to 200% with the addition of 50 wt% wollastonite. The geopolymer composites were exposed to high temperatures at 800°C to 1100°C for 2 h. Cracks were reduced since 20 wt% wollastonite was added. A high percentage of wollastonite presented excellent thermal stability. The total weight loss of the geopolymer composite at temperatures of 30°C to 1400°C was minimized. It decreased from 25% to 12% when 50 wt% wollastonite was added, and the dilatometric data resulted in a dimensional change of almost zero. The phase development of the geopolymer composites at high temperatures showed the crystallization of leucite, kalsilite, calcium silicate, calcium aluminium silicate, and calcium aluminium oxide, which were the high temperature stable phases. The results indicated that wollastonite reinforced fly ash-based geopolymer composites are promising for use in high temperature applications.

## 1. Introduction

Geopolymers are one of the attractive materials and are rapidly becoming well-known for a half-century [1]. The utilization of waste materials in geopolymer synthesis has increased as mounting environmental concerns focus on accumulating a stockpile of industrial by-products. It reduces the global warming problem because it is energy saving and environmentally friendly. Natural and industrial by-product ingredients, such as pozzolanic materials, fly ash, bottom ash, bagasse ash, rice husk ash, and blast furnace slag, are used to produce geopolymers. These have the potential for preparing the geopolymer due to the significant aluminosilicate constituents. It is possible to apply geopolymers in engineering perspectives because of the high early compressive strength and durability, especially a fly ash-based geopolymer that presents properties close to Portland cement [2]. Geopolymers are utilized in various applications, particularly for thermal applications resulting from its inorganic nature, such as refractory, insulating, and fire-resistant products [3]. Many previous studies reported the geopolymer synthesis and properties for high temperature applications. The produced geopolymer always lost its stability during high-temperature exposure [4-7]. The main factors influencing the mechanical strength of a

geopolymer are the shrinkage and microstructure. It resulted from the effect of the Si/Al ratio, alkali cation, and the evaporation of free water and water in the geopolymer structure [8-10]. The most straightforward approach proposed to minimize the shrinkage behavior is by incorporating thermal stability materials into a geopolymer.

There are many materials for geopolymer reinforcement in order to improve the mechanical and thermal properties. Those are particulate and fibrous materials such as Al<sub>2</sub>O<sub>3</sub>, quartz, refractory brick, and fibers [6,9]. Alomayri [11] proposed the inclusion of a glass microfibers in fly ash-based geopolymer. The flexural strength increased at an optimum glass microfiber content of 2 wt%. The flexural strength of the geopolymer composite decreased beyond the optimum reinforcement content because of the fiber agglomeration. A weak inter-facial bond between the fiber and the matrix consequently occurred. Nuaklong *et al.* [12] investigated the mechanical strength of the fly ash-based geopolymer mortar reinforced with carbon fiber. The compressive strength was increased 21% compared with the control when 0.2 wt% carbon fiber was added. Furthermore, the carbon fiber enhanced the flexural strength significantly. The addition of 0.2 wt% to 0.3 wt% carbon fiber could increase the flexural strength up to 54% compared with the control. These resulted from the bridging effect of the fiber. Timakul *et al.* [13] reported the improvement

in the property of a high calcium fly ash-based geopolymer after the addition of basalt fiber. They found that the high Ca/Si ratio in the geopolymer matrix due to the high CaO content in the fly ash raw material resulted in the high compressive strength. The compressive strength was enhanced by 37% when 10 wt% basalt fiber was added compared to the neat geopolymer. However, the compressive strength slightly improved when more than 10 wt% basalt fiber was added. In addition, Timakul *et al.* [14] also prepared a high calcium fly ash-based geopolymer by improving the thermal stability at high temperatures up to 800°C. The geopolymer was reinforced by basalt fiber to enhance the mechanical and thermal properties. The thermal properties of the geopolymer composite were enhanced by adding about 1 wt% to 5 wt% TiO<sub>2</sub>. The thermal shock resistance of the geopolymer with TiO<sub>2</sub> was up to 15 cycles of heating at 800°C. Suthee *et al.* [15] reported the geopolymer-mullite composite synthesized from fly ash and mullite powders. They found that 40% to 60% mullite addition improved the compressive strength from around 58 ± 21 MPa to 72 MPa to 76 MPa due to a needle-like structure of the mullite. The compressive strength decreased after high temperature exposure at 400°C to 1000°C and maintained around 15 MPa. Due to the good mechanical strength, chemical stability, resistance to deformation, and high temperature stability of the geopolymer, it is an alternative material for many applications such as heat and fire resistance, insulating material, coating for fire protection, and refractory [16,17].

Wollastonite (CaSiO<sub>3</sub>) is a natural mineral with an acicular shape and a needle-like or fiber morphology. Its physical properties have several advantages, i.e., mostly inert in a basic condition so that it does not react with other components either during or after the manufacturing process, a high melting point at 1540°C resulting in high temperature stability up to about 1120°C, and a low coefficient of thermal expansion,  $6.5 \times 10^{-6} \text{ }^\circ\text{C}^{-1}$  over a range of 25°C to 800°C [18]. Wollastonite has aspect ratios (the particle length to the particle diameter) varying from 3:1 to 20:1. Consequently, wollastonite is useful as an industrial mineral reinforcement in many applications, such as thermal insulation, refractory, a replacement for asbestos in cement, plastic, paint film, and roofing tile [19-21].

Among the applications, the use of wollastonite to improve the properties of cement is widely studied in order to replace the asbestos in cement and concrete applications [22]. Khan *et al.* [23] reported that cement replaced by 30 wt% ground wollastonite resulted in C<sub>3</sub>S hydration and the acceleration of the reaction of aluminates phases. However, it reduced the compressive strength of the cement mortar mixture. The particle size of wollastonite affected the compressive strength, with a mean particle size lower than 3.5 μm reducing the compressive strength by only 10% after 28 days of curing. Yücel and Özcan [24] studied the synthetic wollastonite replaced cement phase. The mechanical properties of the cement mortar improved with 9 wt% synthetic wollastonite and decreased beyond this replacement value. The acicular particle structure of wollastonite attributed to the microcrack bridging of the cement mortar. Bong *et al.* [25] reported the mechanical strength of fly ash-based geopolymer mortar using wollastonite as fly ash and sand replacement. The wollastonite improved the compressive strength of geopolymer mortar when used as fly ash and sand replacements. The flexural strength was enhanced by wollastonite when using as sand replacement. On the

other hand, it did not improve when used as fly ash replacement because the reduction of fly ash which was the geopolymer precursor resulting in the low geopolymerization. However, there has not been much research done on the utilization of wollastonite in the fly ash-based geopolymer applications, especially in high-temperature applications.

Therefore, the aim of this research was the improvement of thermal stability of the fly ash-based geopolymer by adding the wollastonite fiber. The geopolymer specimens were prepared in the presence of KOH and K<sub>2</sub>SiO<sub>3</sub> as the alkaline activator solution. The mechanical and thermal properties of the cured geopolymer specimens were investigated either before or after exposure to high temperatures. The thermogravimetry/differential thermal analysis (TG/DTA) and dilatometer were employed to analyze the thermal property. Compressive strength and flexural strength tests were applied to determine their mechanical property. The Scanning electron microscopy (SEM), X-ray diffractometer (XRD), and Fourier transform infrared spectroscopy (FT-IR) were used to evaluate the microstructure, phase development, and chemical bonding of the geopolymer, respectively.

## 2. Experimental

Fly ash from Mae Moh power plant at Lampang province in the northern part of Thailand was used as a starting material to prepare the geopolymer in this study. The chemical composition was analyzed by X-ray fluorescence (XRF, S8 Tiger, Bruker, Germany), as shown in Table 1. The main compositions were SiO<sub>2</sub> and Al<sub>2</sub>O<sub>3</sub> incorporated with a high content of CaO, Fe<sub>2</sub>O<sub>3</sub>, and other trace elements. It was classified as class C fly ash in accordance with ASTM C618-03, in which the CaO content was higher than 10%.

Figure 1(a) shows the phase analysis by XRD (X'Pert Pro Diffractometer, Panalytical) composed of anhydrite (CaSO<sub>4</sub>, PDF# 37-1496), lime (CaO, PDF# 37-1497), quartz (SiO<sub>2</sub>, PDF# 46-1045), hematite (Fe<sub>2</sub>O<sub>3</sub>, PDF# 33-0664), maghemite (Fe<sub>2</sub>O<sub>3</sub>, PDF# 39-1346), magnesioferrite (MgSi<sub>2</sub>-<sub>3</sub>O<sub>4</sub>, PDF# 17-0464), and portlandite (Ca(OH)<sub>2</sub>, PDF# 04-0733). The microstructure of fly ash evaluated by SEM (JSM 7800F Prime, JEOL Ltd., Japan) is shown in Figure 2(a). The sample was spherical in shape and showed various sizes with a multi-modal particle size distribution. The mean particle size was 29.8 μm.

Wollastonite fiber was employed as a reinforcement in the geopolymer preparations. The chemical compositions of the wollastonite fiber collected from the manufacturer are shown in Table 1. The main compositions were SiO<sub>2</sub> and CaO. Figure 1(b) shows the phase analysis of wollastonite by XRD, which the primary phase is the wollastonite phase. The microstructure of the wollastonite is presented in Figure 2(b). The fiber shape had a length and diameter of 498 μm and 40 μm, respectively, and the aspect ratio was about 12.

The fly ash-based geopolymer samples were synthesized by mixing class C fly ash and the alkaline activator. The alkaline activator was prepared from potassium hydroxide (95.5 wt% KOH, Nisso, Nippon Soda Co. LTD., Japan), distilled water, and a potassium silicate solution (K<sub>2</sub>SiO<sub>3</sub>, 13.0 wt% K<sub>2</sub>O and 26.9 wt% SiO<sub>2</sub>, C. Thai Chemicals Co., LTD., Thailand).

Firstly, KOH was mixed with distilled water at a 6 M concentration and cooled down by keeping at room temperature overnight before adding the K<sub>2</sub>SiO<sub>3</sub> solution and mixing thoroughly. The KOH and

$K_2SiO_3$  were in a 1:1 weight ratio. Secondly, the geopolymer was synthesized by dry mixing fly ash and wollastonite fiber ranging from 5 wt% to 50 wt% fly ash via a food processor mixer for 3 min. Then, the alkaline activator was poured to the dry solid part, in which the solid to liquid weight ratio was 3:2 and mixed for 90 s by a handheld mixer. The geopolymer mixture was cast into a cube mold, which is  $50 \times 50 \times 50$  mm in size, for the compressive strength testing and a bar mold, which is  $20 \times 20 \times 80$  mm in size, for the flexural strength testing. The hardened specimens were de-molded and wrapped by plastic film to prevent water loss and kept at ambient temperature for 7 and 28 days.

Compressive strength was measured via the cement compression machine (ADR Auto-250, ELE International) with force applied at a rate of  $1.0 \text{ kN}\cdot\text{s}^{-1}$  at 7 and 28 days of curing according to ASTM C109. Flexural strength was carried out by a 3-point bending strength test via a Universal Testing Machine (UTM, Instron 55R4502) at a crosshead speed of  $0.5 \text{ mm}\cdot\text{min}^{-1}$  and a span of 60 mm. Another set of the specimens was subjected to high temperature stability testing at  $800^\circ\text{C}$  to  $1100^\circ\text{C}$  for 2 h with a  $5^\circ\text{C}\cdot\text{min}^{-1}$  heating rate in a furnace after 28 days of curing. The fired geopolymer composites without a noticeable crack were then subjected to the compressive strength test. The thermal properties of the geopolymers and geopolymer composites were analyzed after 28 days of curing.

The TG/DTA technique (NETZSCH STA 449C, NETZSCH) was performed at a temperature of  $30^\circ\text{C}$  to  $1400^\circ\text{C}$  and a heating rate

of  $10^\circ\text{C}\cdot\text{min}^{-1}$  in the air to study the change in the material under high temperatures. The optical dilatometer (ODP868, TA) was employed at a temperature of  $30^\circ\text{C}$  to  $1100^\circ\text{C}$  and a heating rate of  $10^\circ\text{C}\cdot\text{min}^{-1}$  in the air to study the thermal expansion. The phase development was evaluated by XRD (X'PertPro Diffractometer, Panalytical) at  $10^\circ$  to  $70^\circ 2\theta$  with a scanning speed of  $2^\circ\cdot\text{min}^{-1}$ . The SEM (JSM 7800F Prime, JEOL Ltd.) equipped with the Energy Dispersive X-ray Spectroscopy (EDS) apparatus was applied to investigate the microstructure and chemical composition. The chemical bonding of the geopolymer was identified by FT-IR (Perkin Elmer System 2000) from  $400 \text{ cm}^{-1}$  to  $4000 \text{ cm}^{-1}$  with the KBr pellet technique.

**Table 1.** Chemical compositions of the raw materials.

Chemical	Component (%)	
	Fly ash	Wollastonite
$\text{SiO}_2$	34.05	49.06
$\text{Al}_2\text{O}_3$	18.17	0.99
CaO	21.31	45.72
$\text{Fe}_2\text{O}_3$	13.87	1.44
$\text{Na}_2\text{O}$	1.69	0.019
$\text{K}_2\text{O}$	2.60	0.019
MgO	2.01	0.13
$\text{SO}_3$	5.09	-
Others	1.01	2.62
LOI	0.17	3.20

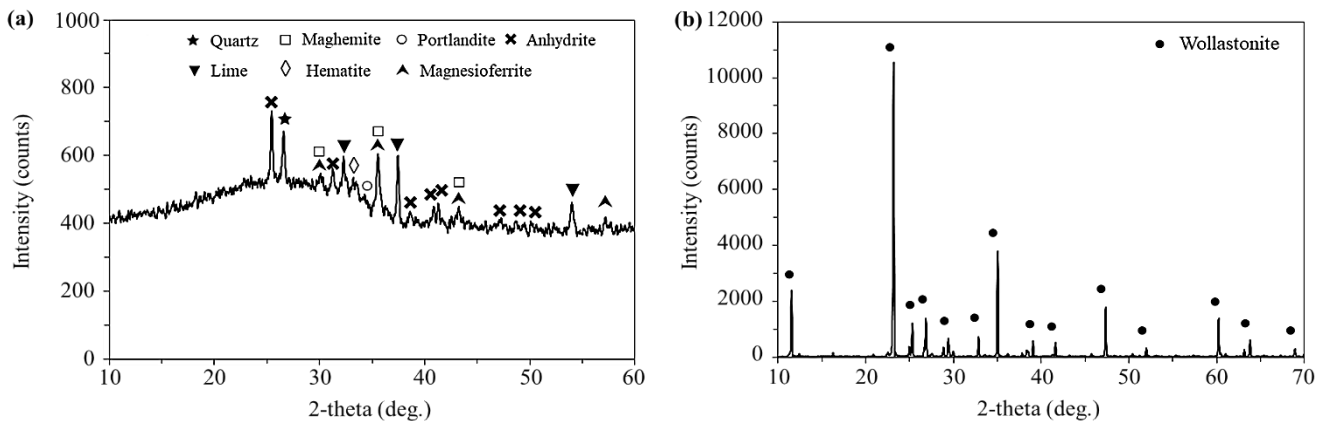


**Figure 1.** XRD patterns of (a) fly ash and (b) wollastonite.

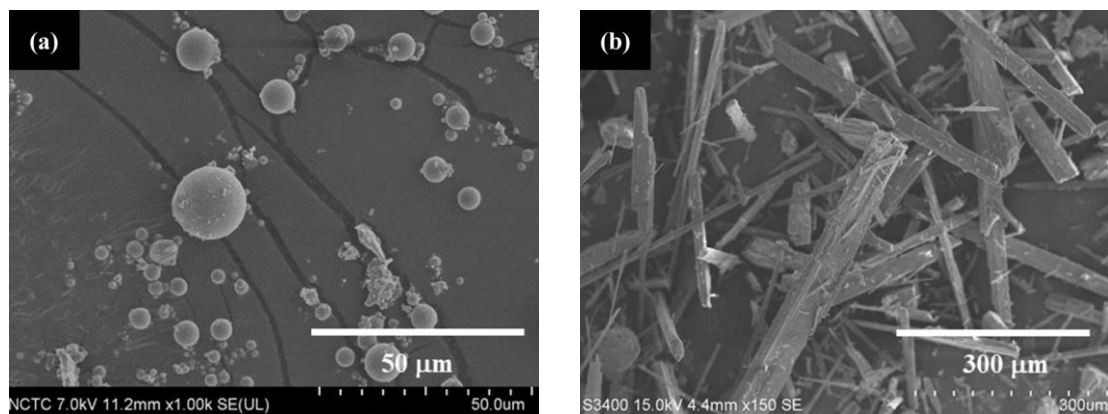


**Figure 2.** SEM micrographs of (a) fly ash and (b) wollastonite.

### 3. Results and discussion

#### 3.1 Mechanical strength

The mechanical properties of the geopolymer and geopolymer composites that were reinforced by various amounts of wollastonite are presented in Figure 3 and Figure 4. It can obviously be seen that the mechanical properties improved by adding wollastonite. Figure 3 shows the compressive strength of the geopolymer and geopolymer composites. The compressive strength of the geopolymer without reinforcement at 7 days was 17.2 MPa and it increased about 2 times, 33.3 MPa when the prolonged curing time increased from 7 days to 28 days. The maximum compressive strength was about 23.4 MPa and 38.4 MPa with 30 wt% to 40 wt% wollastonite when the curing time was 7 days and 28 days, respectively.

Typically, construction applications require a construction brick with a compressive strength of 25 MPa to 40 MPa at 28 days of curing [26]. Therefore, these geopolymer composites appear to be potential materials for construction bricks. Nevertheless, a higher amount of wollastonite no longer contributes to the development of the compressive strength. Under compression, the geopolymer is destroyed by the formation of microcracks in the opposite side of the compression load, and then, the crack propagates because of the concentration of tensile stress in front of the broken part. The geopolymer containing the fiber demands a high energy of fracture to enlarge the crack and pull out the fiber for propagation because the fiber acts as the microcracks bridging [27]. However, this also depends on the interaction between the fiber and matrix, the type and amount of fiber, and the fiber dispersion in the matrix. As a result, the wollastonite fiber presented the inert characteristic in the basic solution; hence, the large amount of wollastonite has an insignificant effect on the compressive strength.

Conversely, the addition of wollastonite was found to have a positive effect on the flexural strength, as presented in Figure 4. The flexural strength was more developed when prolonging the curing time to 28 days and successively increasing the wollastonite content. The relative flexural strength was also calculated in comparison to the geopolymer to point out that the wollastonite improved the flexural strength remarkably. The flexural strength at 7 days of the geopolymer without reinforcement was 1.1 MPa and it increased to 2.1 MPa at 28 days of curing. Moreover, the maximum flexural strength of 6.8 MPa was obtained at 28 days of curing when 50 wt% wollastonite was added. The relative flexural strength increased by about 200%. Therefore, this result can be explained by the fibrous nature of wollastonite exhibiting a crack deflection behavior of fiber-matrix composites [28].

There have been previous studies supporting the improvement in the mechanical strength by adding wollastonite to cementitious materials. Archez *et al.* [29] revealed that a wollastonite filler improved the viscosity and mechanical properties of the geopolymer composites. The addition of wollastonite enhances the compressive strength, with the failure mode becoming ductile with a higher wollastonite content. It might be described by the acicular shape of wollastonite modifying the microstructure of the geopolymer. This behavior was similar to the wollastonite powder replaced cement or sand performed

by Wahab *et al.* [19] Their study revealed the mechanical properties of cement mortar mixes, with the cement or sand being replaced by wollastonite powder. The compressive strength and flexural strength increased with the wollastonite replacing the sand content; however, both results decreased when the wollastonite amount was more than 20 wt%. In contrast, the mechanical strength saw little improvement when wollastonite replaced the cement content. It drastically decreased when cement was replaced with the wollastonite powder due to the reduction of the cementitious phase.

In addition, Yücel and Özcan [24] studied the replacement of cement with 3 wt% to 15 wt% synthesized wollastonite and reported that the increased content of synthetic wollastonite increased the compressive strength and flexural strength. However, after substitution with 9 wt% wollastonite, the mechanical strength of the cement mortar started to decline. Similarly, Alomayri [11] revealed the effect of glass microfibers on the reinforcement of a fly ash-based geopolymer. The flexural strength of the geopolymer increased with the increase in the glass microfibers from 1 wt% to 2 wt%, although it declined when a higher amount of glass microfibers was added. Additionally, the result showed that the high viscosity of the geopolymer mixtures obtained from the addition of 3 wt% glass microfibers prevented the development of the flexural strength.

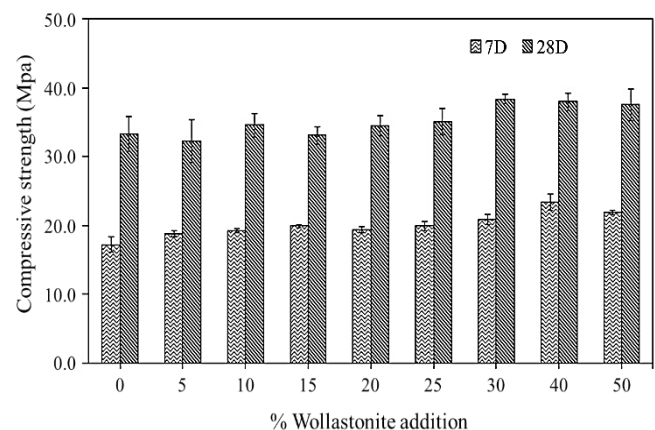


**Figure 3.** Compressive strength of the geopolymer composites with various amounts of wollastonite at 7 days and 28 days of curing.

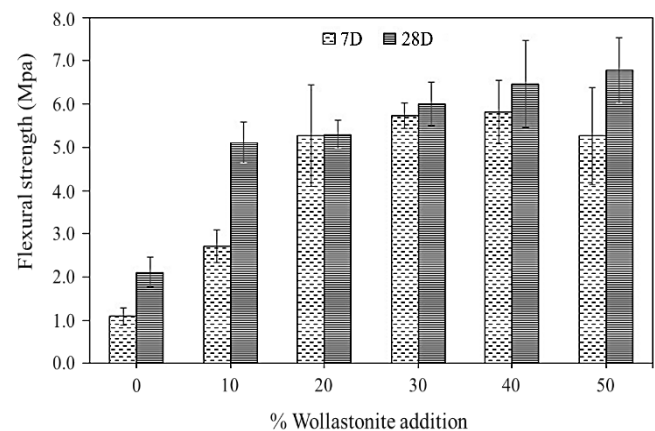


**Figure 4.** Flexural strength of the geopolymer composites with various amounts of wollastonite at 7 days and 28 days of curing.

However, the compressive strength and the flexural strength slightly decreased when more than 40 wt% wollastonite fiber was added. This might result from the effect of the solid to the liquid ratio of the geopolymer mixture. The addition of the wollastonite increased the solid to liquid ratio from 1.5 to 2.25 such that the mixture was difficult to mix and cast. The effects of excessive reinforcement could be considered because the inert reinforcement might inhibit the geopolymer network structure, causing the decline in the mechanical strength. One of the reasons for the reduction of the flexural strength is because of a non-homogeneous geopolymer mixture. It can be described that the homogeneous geopolymer matrix of the composite can be obtained with a low fiber addition, and thus, the much higher tensile strength of the fiber is considered to increase the flexural strength of the composite [30]. Furthermore, the high fiber content resulted in the poor compaction of the fresh mixture due to the high solid to liquid ratio. Then, the heterogeneous fiber-matrix interaction may occur and cause the porous structure formation. That caused the deficient interfacial adhesion of the microfiber and geopolymer matrix and the consequent reduction in the flexural strength when the fiber content is high. However, the time of curing was also considered due to its influence on the strength development. The flexural strength of the high fiber reinforced was more developed at 28 days of curing. Therefore, the type and content of the reinforcement for each fiber could be optimized to obtain the optimum mechanical properties.

### 3.2 FT-IR analysis

Figure 5 presents the FT-IR spectra of the geopolymer and geopolymer composites reinforced by various amounts of wollastonite fiber at 28 days of curing comparing to fly ash and wollastonite. The characteristic absorption band of all the geopolymer and geopolymer composites attributed to the asymmetric stretching vibration of Si-O-Si and Al-O-Si is shifted from that of the original fly ash. In the original fly ash, this band appeared as a broad band with two peaks at 1098  $\text{cm}^{-1}$  and 1002  $\text{cm}^{-1}$ . It became narrower and moved to a lower wavenumber around 960  $\text{cm}^{-1}$  to 1000  $\text{cm}^{-1}$  for the geopolymer due to the substitution of the  $[\text{AlO}_4]^{3-}$  groups in the  $[\text{SiO}_4]^{4-}$  groups by the alkaline activation as a result of the geopolymerization reaction [31,32].

In addition, the geopolymer composites containing more wollastonite exhibit a peak shifted to lower energy, from 995  $\text{cm}^{-1}$  to around 968  $\text{cm}^{-1}$  to 972  $\text{cm}^{-1}$ . These seem to be a possible result of the incorporation of a tetrahedral coordination framework of calcium cations, which increase the bond length and decrease the bond angle of T-O-Si [33,34]. The vibration band appears as the shoulder located at 1100  $\text{cm}^{-1}$  to 1160  $\text{cm}^{-1}$  representing the formation of  $[\text{SO}_4]^{2-}$ . It is the asymmetric stretching vibration of S-O that also is found in cement [35].

The intense vibration band at 454  $\text{cm}^{-1}$  reflected the bending vibration of O-Si-O persisting in the geopolymer and geopolymer composites due to the lower reaction of quartz in the alkaline activation [36,37]. The band located at 595  $\text{cm}^{-1}$ , 611  $\text{cm}^{-1}$ , and 678  $\text{cm}^{-1}$  of fly ash represented the symmetric stretching vibration of Si-O-Si and Al-O-Si that were the silicate and aluminosilicate glasses possessing a long-range order structure in the form of tetrahedral or octahedral rings [7,38].

The new band at 1410  $\text{cm}^{-1}$  to 1450  $\text{cm}^{-1}$  found in the geopolymer is attributed to the stretching vibration of O-C-O due to the presence of high calcite [14,35]. The band appearing at 1644  $\text{cm}^{-1}$  and the broad region centered at around 3437  $\text{cm}^{-1}$  are assigned to the bending vibration and stretching vibration of the hydroxyl group, respectively. This hydroxyl group was absorbed in the surface and entrapped in pores or the large cavity of the geopolymer structure.

The infrared spectra of the geopolymer composite with high wollastonite content presented closely the vibration band to the vibration band of the original wollastonite, where the broad geopolymer characteristic band was presented. Moreover, the broader peak was obviously seen when more wollastonite fiber was added due to the geopolymer composite containing multiple overlapping components corresponding to the study of Siyal *et al.* [39]. The broad peak of the original wollastonite occurred around 900  $\text{cm}^{-1}$  to 1083  $\text{cm}^{-1}$  indicating the asymmetric stretching vibration of Si-O-Si. The band at the low wavenumber located at 450  $\text{cm}^{-1}$  and 566  $\text{cm}^{-1}$  represented the bending vibration of Si-O and the stretching vibration of Ca-O, respectively [40]. Therefore, it can be summarized that the wollastonite has presented a disperse phase to the geopolymer matrix with less chemical reaction, resulting in a small improvement in the compressive strength as described in 3.1.

### 3.3 XRD analysis

Figure 6 shows the XRD patterns of the geopolymer and geopolymer composites reinforced by various amounts of wollastonite fiber at 28 days of curing. From the XRD results, the geopolymer revealed the characteristic broad hump of the geopolymer, which was an amorphous phase centered at about  $28^\circ$  to  $30^\circ$   $2\theta$  incorporated with the reaction product phases i.e., arcanite ( $\text{K}_2\text{SO}_4$ , PDF# 05-0613), calcium silicate hydrate (C-S-H, PDF# 33-0306), and calcite ( $\text{CaCO}_3$ , PDF# 47-1743) and the remaining crystalline phases from the original fly ash i.e., quartz ( $\text{SiO}_2$ , PDF# 46-1045) and magnesioferrite ( $\text{MgSi}_{2-3}\text{O}_4$ , PDF# 17-0464). According to the Ordinary Portland Cement (OPC) reaction, which is the hydration reaction, calcium is strongly reacted with silicon and aluminium to form various phases of calcium silicate hydrate and calcium aluminate hydrate.

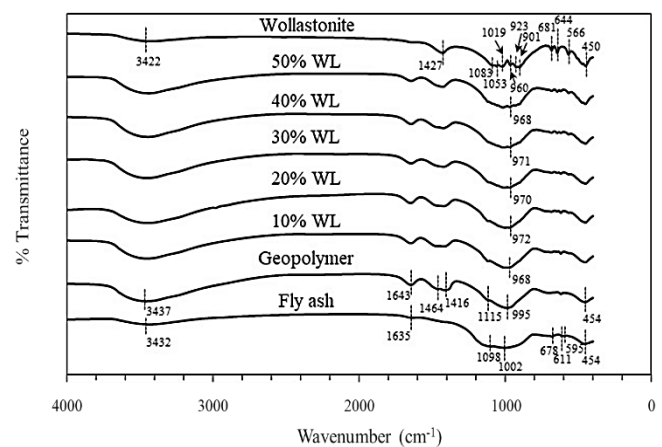


**Figure 5.** FT-IR spectra of the geopolymer and geopolymer composites with 10 wt% to 50 wt% wollastonite (WL) at 28 days of curing compared to fly ash and wollastonite.

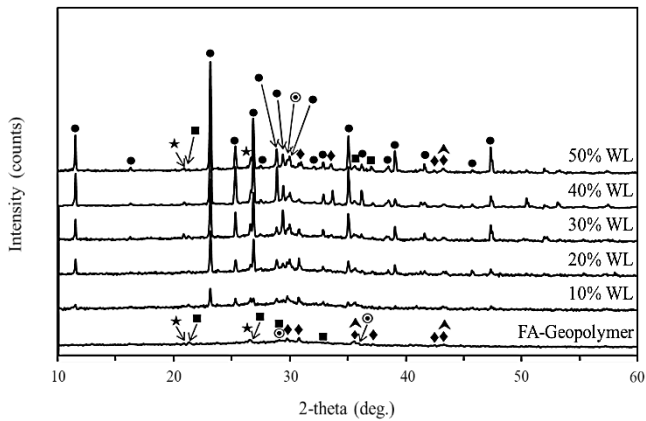


**Figure 6.** XRD patterns of the geopolymer and geopolymer composites at 28 days of curing [● wollastonite ( $\text{CaSiO}_3$ ), ★ quartz ( $\text{SiO}_2$ ), ⊙ calcite ( $\text{CaCO}_3$ ), ◆ arcanite ( $\text{K}_2\text{SO}_4$ ), ▲ magnisioferrite ( $\text{MgFe}_{2.3}\text{O}_4$ ), ■ calcium silicate hydrate].

Similarly, there was a calcium silicate hydrate phase occurring in the geopolymer due to the reaction of calcium present in the original fly ash, which was the class C fly ash and the soluble silicate in the alkaline activator [41]. In addition, the presented calcium obviously affected the setting time of the class C fly ash-based geopolymer [42].

The XRD patterns of the geopolymer composites reinforced by various amounts of wollastonite fiber showed the wollastonite phase ( $\text{CaSiO}_3$ , PDF# 43-1460) coexisting with the phases found in the fly ash-based geopolymer. The intensity of the wollastonite

phase increased with the increase in the wollastonite content. The broad hump of the amorphous geopolymer still occurred whenever the wollastonite fiber increased. The wollastonite exhibits good chemical stability. It does not react with the environment, especially in a basic solution [18]. Consequently, new reaction phases did not occur; this infers that the improved mechanical strength is resulting from the wollastonite morphology and content.

### 3.4 SEM analysis

Figure 7 shows the microstructure of the geopolymer and geopolymer composites examined on the fracture surfaces of the compressive strength testing specimens by SEM. The morphology of the geopolymer in Figure 7(a) shows dense structures and some long cracks. The cracks might be formed during specimen breaking rather than during the curing and drying process. The presented dense structure was a geopolymer matrix with an Si/Al of 2.4 compared to the original fly ash particle with an Si/Al of 1.4, according to the EDS analysis as shown in Figure 8. It infers that fly ash was activated by the alkaline activator and forms the geopolymer phase related to the XRD and FT-IR results. The geopolymer microstructure not only revealed the geopolymer matrix part but also presented other reaction products, non-completely reacted fly ash particles, and unreacted fly ash particles that were embedded in the geopolymer matrix. According to the XRD results, the major reaction products were arcanite, calcite, and calcium silicate hydrate.

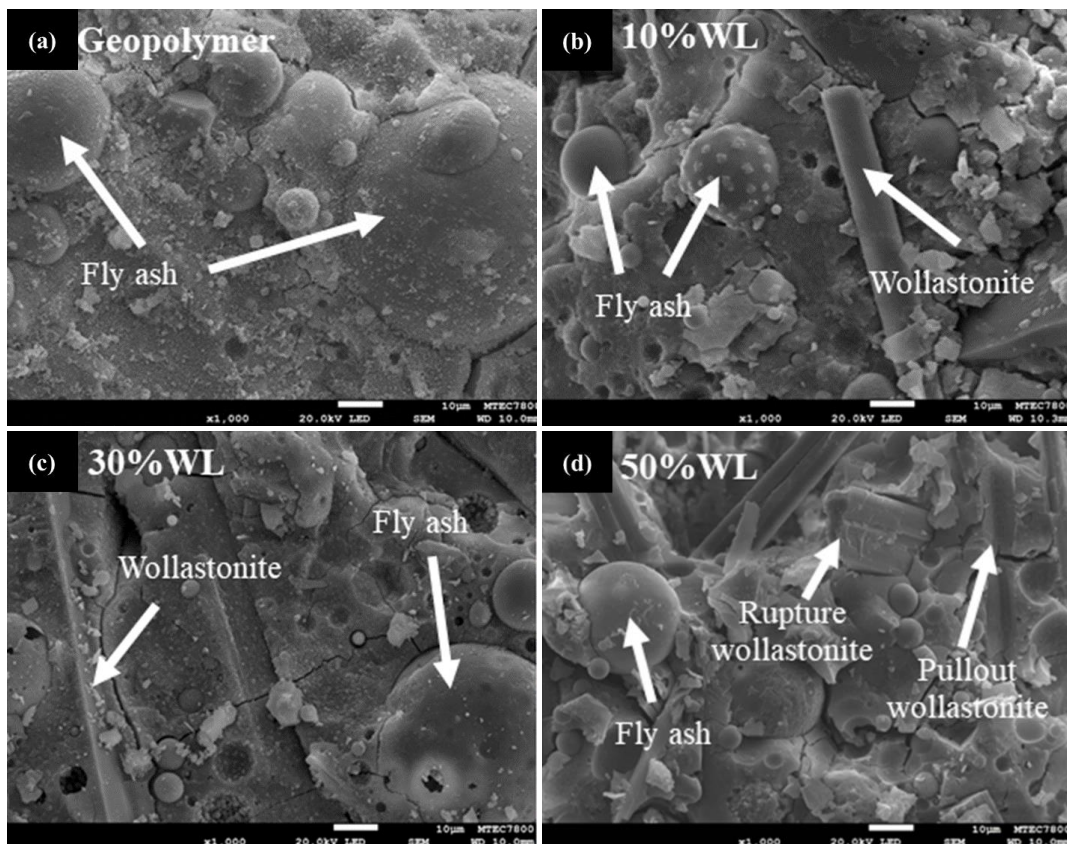


**Figure 7.** Microstructure of (a) geopolymer and geopolymer composites with (b) 10 wt%, (c) 30 wt%, and (d) 50 wt% wollastonite.

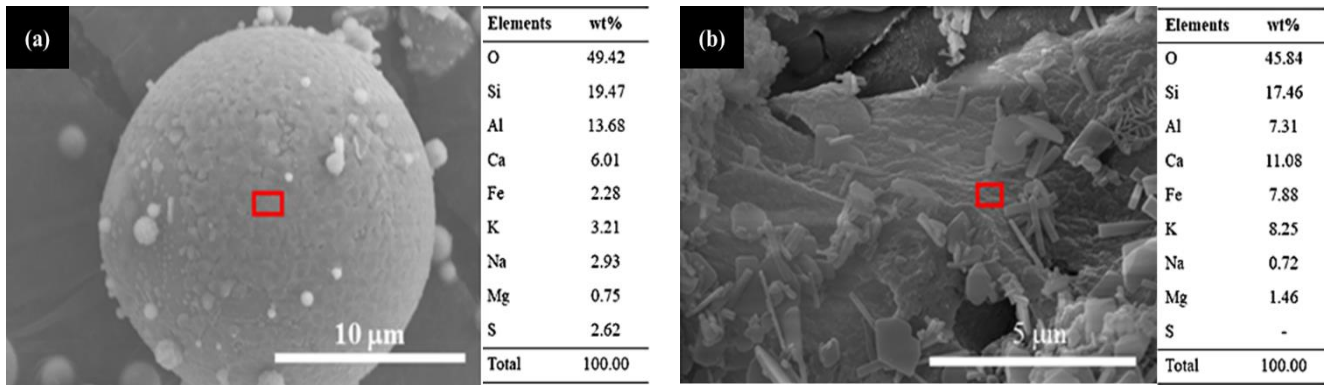


Figure 8. EDS analysis of (a) original fly ash and (b) geopolymer.

In comparison, the geopolymer composites reinforced by wollastonite fiber at 10 wt%, 30 wt%, and 50 wt%, respectively, were chosen to evaluate the microstructure, as presented in Figure 7(b)-(d). The geopolymer matrix part appeared to have a similar microstructure to the geopolymer without wollastonite, but there were wollastonite fibers that were embedded in the geopolymer matrix. The geopolymer composite microstructure showed some of the smooth surface fibers, suggesting that there was poor bonding of the wollastonite fibers to the geopolymer matrix due to the basic solution resistance of wollastonite.

The evidence of the attachment of the geopolymer matrix and wollastonite fibers was presented in Figure 7(c). The rupture and pullout of wollastonite fibers were observed, as shown in Figure 7(d). These results reflect the effect of the wollastonite fiber on the flexural strength. Although, the wollastonite fibers occur the weak bonding to the geopolymer matrix, the flexural strength appears to be increased by more than 200% because of its fibrous microstructures. Similarly, Kwon *et al.* [23,43] reported that the microstructure of wollastonite microfibers improved the mechanical properties of cement. There was the hydration reaction occurring at the interface of the cement and wollastonite, which was the microfiber-matrix interfacial bonds to form the C-S-H phase. Therefore, the microstructure was favorable for improving the flexural strength, which was mostly comprised of the rupture, pullout, and adhesion of the fiber-matrix interface.

### 3.5 Compressive strength after high temperature exposure

Compressive strength is an important property that plays an essential role in all geopolymer applications. The fly ash-based geopolymer with an optimum preparation condition gives a high compressive strength at ambient temperature, although it lacks stability when exposed to high temperatures. The appearance of those geopolymer specimens after firing at 800°C and 1000°C is shown in Figure 9. It is noticeable that severe cracks occurred at high temperatures, causing these geopolymers to be too weak to measure their compressive strength. It is well known that the shrinkage and cracking of the geopolymer result from water loss over time by evaporation during heating. The insufficient durability at high temperatures corresponded to the repulsion of water in the small pores and structure, causing the partial collapse in the geopolymer structure [44]. Therefore, wollastonite was chosen as the thermally stable filler to maintain the properties at the optimum value.

The geopolymer specimens were exposed to high temperatures of 800°C to 1100°C for 2 h and a 5°C·min<sup>-1</sup> heating rate. Figure 10(a) shows the appearance of geopolymer composites after thermal treatment at 800°C. There were visible cracks on the specimen surfaces that contained 0 wt% to 15 wt% wollastonite. The crack was gradually reduced when the wollastonite was increased and eventually disappeared when the wollastonite was increased more than 20 wt%. It was eliminated when the wollastonite was added beyond these amounts. Figure 10(b) presents the geopolymer composite with 40 wt% wollastonite after exposure to high temperatures, 800°C to 1100°C. The specimens maintained their shapes without cracking at those high temperatures. It implied that the geopolymer composite with wollastonite was stable at high temperatures.

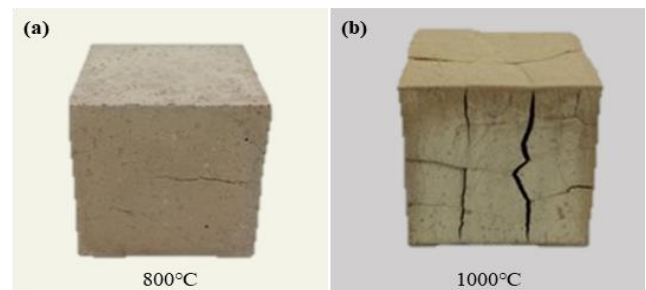


Figure 9. Geopolymer specimens after high temperature exposure, (a) 800°C, and (b) 1000°C.

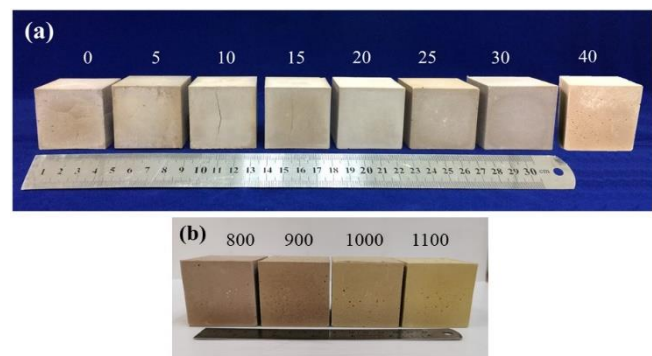


Figure 10. Appearance of the geopolymer composites with (a) 0 wt% to 40 wt% wollastonite after exposure to 800°C, and (b) 40 wt% wollastonite after exposure to high temperatures.

Figure 11(a) illustrates the compressive strength of the geopolymer and geopolymer composites after 28 days of curing and after exposure to 800°C to 1100°C for 2 h. As aforementioned, the geopolymer lost its strength at high temperatures, the compressive strength was less than 2 MPa after exposure to 800°C. The geopolymer composite specimens contained wollastonite less than 20 wt% were not strong enough to be subjected to the compression test after exposure to temperature of 800°C to 1100°C. Therefore, the compressive strength of the thermally stable geopolymers was carried out on only geopolymer composites reinforced with 20 wt% 50 wt% wollastonite because they were tolerated, and no visible cracks were observed at high temperatures.

The compressive strength of geopolymer composite with 50 wt% wollastonite was decreased from about 37.5 MPa to 6.4 MPa after exposure to 1000°C. Although the compressive strength of all geopolymer composites decreased drastically upon heating to high temperatures, these geopolymer composites showed higher residual compressive strength than the controlled geopolymer. The residual compressive strength increased with the addition of wollastonite; it was more than 5 MPa when 40 wt% to 50 wt% wollastonite was added.

Furthermore, the compressive strength after firing compared to non-firing was indicated as the relative residual compressive strength. Figure 11(b) shows the relative residual compressive strength, which is the ratio calculated from the compressive strength after firing and the compressive strength of each composition at 28 days of curing [45]. The relative residual compressive strength of the geopolymer without reinforcement decreased with increasing temperature. It was eventually destroyed at 1000°C where the compressive strength could not be determined. On the other hand, the relative residual compressive strength of the geopolymer composites increased with increasing wollastonite content. The maximum value was up to 20% at 1100°C when 50 wt% wollastonite was added. It infers that the strength reduction of the geopolymer after high temperature exposure resulting from the internal fracture occurred due to the different thermal stresses between the outer and the inner surface during firing. The internal crack took place due to the outer surface contracting, and the internal stress was developed upon heating, which damaged the geopolymer structure. For a better understanding

of the thermal stability of the geopolymer, the optical dilatometer was applied to evaluate the dimensional changes of the geopolymer during heating up to 1100°C.

### 3.6 Thermal expansion analysis

Figure 12 shows the dilatometric curves of the geopolymer and geopolymer composites with 30 wt% and 50 wt% wollastonite at 28 days of curing. The thermal deformation of the geopolymer differed from the geopolymer composites. The geopolymer without reinforcement presented significant shrinkage of about 1.0% at the temperature ranging from 90°C to 250°C due to the dehydration of free water. The shrinkage occurred sharply until 250°C that involved the evaporation of water trapped in the pores resulting in the partial collapse of the pores when the solution in the pores was removed.

At 250°C to 650°C, the geopolymer dimension was slightly contracted due to the hydroxyl group being slowly dehydroxylated, which is associated with the pore structure changes because the water was removed. The minimum dimensional change occurred in this temperature range. Moreover, the release of water caused the compaction of the structure from the condensation of hydroxyl groups on the surface of the geopolymer gel, resulting in the creation of a T-O-T linkage where T is a silicon or aluminium atom [37,46]. A shrinkage of about 1.5% obviously occurred at a temperature of 650°C to 900°C, which was involved in the sintering and densification of the geopolymer gel. At this temperature range, the viscous flux and viscous sintering of the geopolymer matrix occurred, where the viscous flux filled the pores and voids in the geopolymer. This was due to the viscous glass-like behavior of the geopolymer, which implied the glass transition temperature ( $T_g$ ) of the geopolymer.

The small expansion was observed when a further high temperature was applied, over 900°C. The expansion after the sintering and densification region might result from the crack formation, some crystallization of the geopolymer phases, an increase in porosity, or a combination of the reasons mentioned above. These results corresponded to the appearance of the fly ash-based geopolymer, as shown in Figure 9, in which the large cracks appeared on the geopolymer surface.

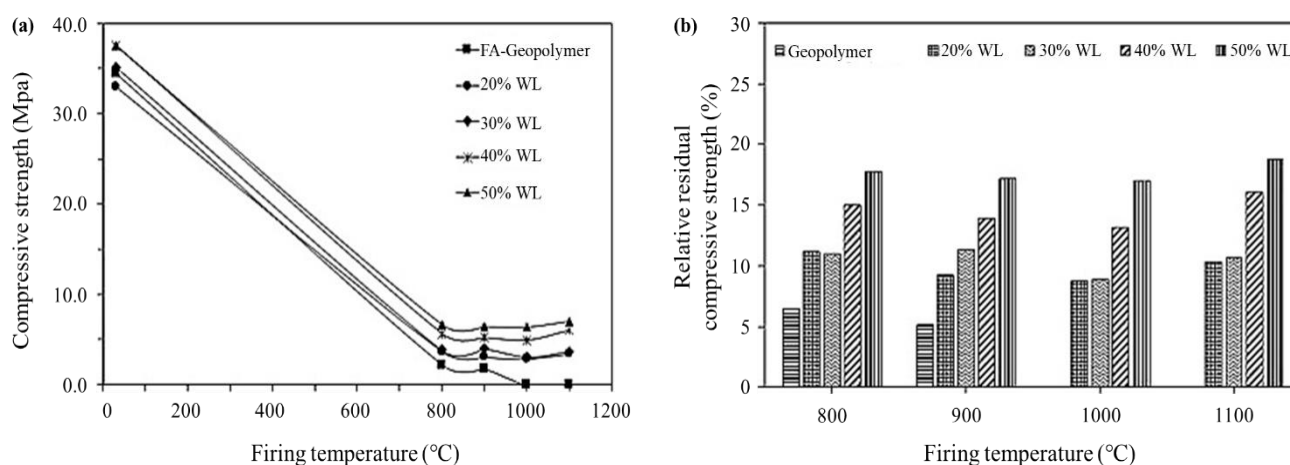


**Figure 11.** (a) Compressive strength, and (b) relative residual compressive strength of the geopolymers and geopolymer composites after exposure to 800°C to 1100°C.

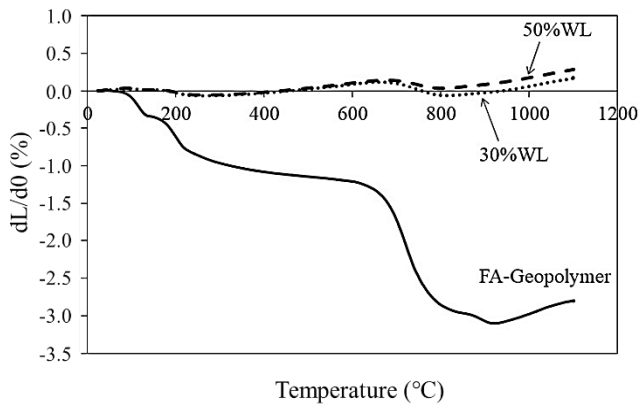


**Figure 12.** Dilatometric data of the geopolymer and geopolymer composites.

Comparing the thermal property of the geopolymer composite to the controlled geopolymer in Figure 12, the overall shrinkage of the geopolymer composites was particularly improved by the wollastonite reinforcements. The 30 wt% and 50 wt% wollastonite present the same thermal expansion behavior. The first shrinkage was found at 150°C to 250°C, which is related to the free water loss. The shrinkage was reduced by 95%, which was lower than the controlled geopolymer. It decreased from 1.0% to 0.05% when 30 wt% 50 wt% wollastonite was added. Based on this evidence, high wollastonite content results in a high solid-to-liquid mass ratio and reflects the smallest overall shrinkage. The minute thermal expansion is exhibited beyond 250°C; that plateau occurred until 700°C with the thermal expansion of 0.14%. However, the thermal expansion behavior was significantly smaller than observed in the controlled geopolymer.

This small expansion was also obtained by Vicker *et al.* [10] on a fly ash-based geopolymer reinforced with alumina and wollastonite. The alumina and wollastonite fillers exhibited the plateau until the temperature rose to 700°C, and this plateau was extended up to 15°C depending on the filler addition. Accordingly, the thermal resistance was increased with the addition of ceramic powder. The second shrinkage was found at 700°C to 800°C, in which the geopolymer phase was sintered, and densification occurred. Similarly, the small thermal expansion also occurred at high temperatures beyond 800°C, while the large cracks did not appear, and the geopolymer was not damaged. It corresponded to the appearance of the geopolymer

composites, as shown in Figure 10. As a result, the dilatometric curve of the geopolymer composite exhibited a lower thermal expansion than the controlled geopolymer.

### 3.7 Thermogravimetric and differential thermogravimetric analysis

Figure 13 presents the thermogravimetric analysis (TGA) and differential thermogravimetry (DTA) curves of the geopolymer and geopolymer composites. The TGA curve, Figure 13(a), shows the weight loss of all geopolymers up to 1400°C. The first weight loss started and proceeded until the temperature reached 200°C, which is related to free water removal that was adsorbed at the surface and in the pores of the geopolymer. The hydroxyl groups in the silicate and aluminates structure were then removed at a temperature ranging from 200°C to 500°C, resulting in the slow continuous weight loss [47,48]. The resulting weight loss was 22% for the geopolymer. It was reduced to 8% and 11% when 30 wt% and 50 wt% wollastonites were added at the similar temperature range due to the increasing solid to liquid ratio. Accordingly, the overall geopolymer weight loss under a temperature up to 500°C mainly corresponded to the dehydroxylation.

The second and third weight loss were found at 500°C to 900°C and 1000°C to 1200°C, respectively. It was determined to be lower than 2% for all geopolymers. The total weight loss at 1400°C of the geopolymer and geopolymer composites reinforced with wollastonite of 30 wt% and 50 wt% were 25%, 13%, and 12%, respectively.

That corresponded to the DTA curves in Figure 12(b), which showed the remarkable endothermic peaks centered at 140°C for the geopolymer and 120°C for the geopolymer composites. The latter presents at lower temperatures due to the smaller water content and compact structure. The next endothermic peak took place at 440°C. It was the lowest intensity of all geopolymers, correlated with the dehydration of  $\text{Ca}(\text{OH})_2$  due to the high calcium content of the fly ash raw material [47]. The broadened endothermic peaks that occurred at around 700°C to 1100°C represented the viscous sintering of the geopolymer phase. In addition, the distinct endothermic peaks were observed at 700°C and 710°C when 30 wt% and 50 wt% wollastonite were added. That might refer to the decarbonation of  $\text{CaCO}_3$  due to the high calcium content in the geopolymer compositions, which is almost generally found in cement upon heating [47,49].

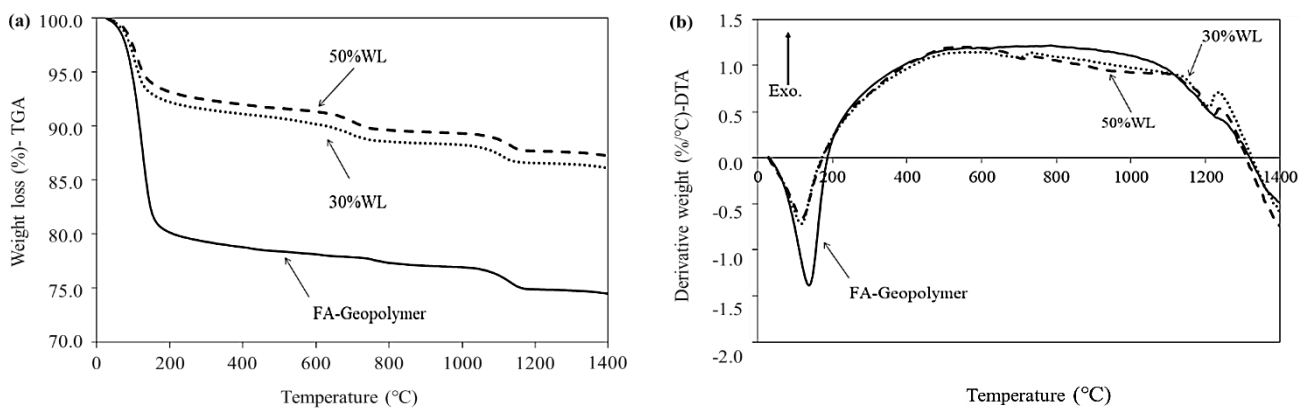


**Figure 13.** (a) TGA, and (b) DTA data of the geopolymer and geopolymer composites.

Above 1200°C, another endothermic peak transformation occurred, which is related to the crystallization during heating, and product phases such as leucite ( $K_2O \cdot Al_2O_3 \cdot 4SiO_2$ ) and kalsilite ( $K_2O \cdot Al_2O_3 \cdot 2SiO_2$ ) were formed [47]. The evidence of phase transformation of the geopolymer and geopolymer composite after exposure to high temperatures was shown in Figure 14 and Figure 15.

### 3.8 XRD analysis after high temperature exposure

The XRD technique was applied to the non-fired geopolymers and the fired geopolymers that were fired at temperatures from 800°C to 1100°C, as presented in Figure 14. The crystalline phases of the non-fired geopolymer reflected the fly ash starting material, as described before in Figure 6. There were the phases of quartz, calcite, arcanite, magnesioferrite, and calcium silicate hydrate.

After firing, the characteristic amorphous broad hump of the geopolymer was not noticeable since 800°C, but some crystalline phases, which were found in the non-firing geopolymer, still occurred i.e., quartz and magnesioferrite. The significant peaks that appeared at the temperature range between 800°C and 900°C were gehlenite ( $Ca_2Al_2SiO_7$ , PDF# 35-0755), kalsilite ( $KAlSiO_4$ , PDF# 11-0579), potassium aluminium silicate ( $K_4Al_2Si_2O_9$ , PDF# 50-0437), mayenite ( $Ca_{12}Al_{14}O_{33}$ , PDF# 09-0413), potassium iron oxide ( $K_2FeO_4$ , PDF# 25-0652), and calcium iron oxide ( $CaFe_4O_7$ , PDF# 35-1277). These phases were more developed in the geopolymer when increased the firing temperature to 1100°C.

In addition, there were new phases appearing at this high temperature, which were leucite ( $KAlSi_2O_6$ , PDF# 38-1423), augite ( $CaFeSi_2O_6$ , PDF# 24-0201), andradite ( $Ca_3Fe_{2+3}(SiO_4)_3$ , PDF# 10-0288), vuagnatite ( $CaAlSiO_4(OH)$ , PDF# 29-0289), wollastonite ( $CaSiO_3$ , PDF# 43-1460), tricalcium aluminate ( $Ca_3Al_2O_6$ , PDF# 38-1429), and calcium aluminate oxide ( $Ca_2Al_2O_5$ , PDF# 01-0572).

In the previous study, the amorphous geopolymer tended to develop crystallinity phases starting from 800°C [50]. The XRD patterns of the potassium based geopolymer after exposure to high temperatures demonstrated that the leucite ( $KAlSi_2O_6$ ), kalsilite ( $KAlSiO_4$ ), and kaliophilite ( $KAlSiO_4$ ) occurred in an amorphous matrix whose intensity increased with temperature [6,51]. Although these phases were the high temperature stable phase, the development of crystalline phases also caused the densification resulting in the large shrinkage, as shown in Figure 12, and destroyed the specimens, as shown in Figure 9. The damage of the geopolymer might be caused by the presence of a high calcium content of the original fly ash, resulting in the C-S-H formation in the geopolymer. The C-S-H shrank rapidly at 500°C and occurred the phase transformation from C-S-H to  $\beta$ - $CaSiO_3$  at 800°C to 900°C [52,53] which might be the one reason for the loss of mechanical strength of the geopolymer. Furthermore, the major reaction was the de-carbonation of calcite at a temperature around 800°C to form free lime, which is ready to react with any accessible ion to form various compound phases of cement, i.e., mayenite, tricalcium aluminate, and calcium aluminate oxide [49]. Therefore, the new crystalline peaks of the geopolymer were formed via the reaction of calcium ions with other available ions, while the amorphous hump of the geopolymer was lost, and some crystalline peaks were also unobserved when exposed to high temperatures.

A comparison of the XRD patterns of the geopolymer and geopolymer composites reinforced with 30 wt% and 50 wt% wollastonite after firing at 1000°C is illustrated in Figure 15. Some phases found in the geopolymer also appeared in the geopolymer composites, which were quartz, gehlenite, kalsilite, and potassium aluminium silicate. The significant peak occurring in the geopolymer composites was wollastonite that was reflected from the filler addition. Calcium silicate ( $Ca_2SiO_4$ , PDF# 49-1672) was a new crystalline phase that might be the reaction product phase of the wollastonite and geopolymer matrix. As seen in Figure 10, the geopolymer composites reinforced with 30 wt% and 50 wt% wollastonite can maintain their shape after high temperature exposure. It can be summarized that the thermal stability of the geopolymer composite was found to be influenced by not only the fiber nature and amount of the wollastonite reinforcement phase but also by the presence of crystalline phases after high temperature exposure.

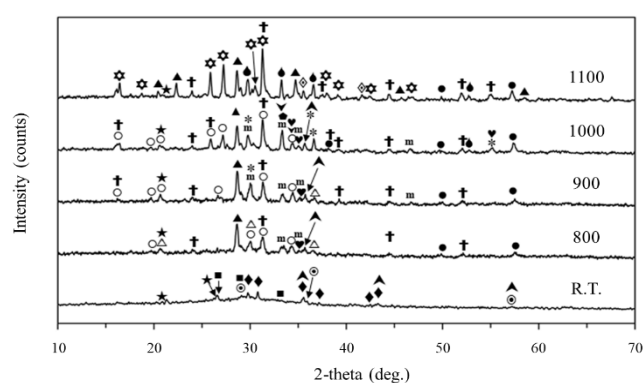


**Figure 14.** XRD patterns of the geopolymer after 28 days of curing at room temperature and after high temperature exposure [ $\square$  arcanite ( $K_2SO_4$ ),  $\blacksquare$  calcium silicate hydrate,  $\star$  quartz ( $SiO_2$ ),  $\odot$  calcite ( $CaCO_3$ ),  $\blacktriangle$  magnesioferrite ( $MgFe_2O_4$ ),  $\dagger$  gehlenite ( $Ca_2Al_2SiO_7$ ),  $m$  mayenite ( $Ca_{12}Al_{14}O_{33}$ ),  $\blacktriangle$  kalsilite ( $KAlSiO_4$ ),  $\star$  leucite ( $KAlSi_2O_6$ ),  $\circ$  potassium aluminium silicate ( $K_4Al_2Si_2O_9$ ),  $\blacktriangledown$  calcium iron oxide ( $CaFe_4O_7$ ),  $\triangle$  potassium iron oxide ( $K_2FeO_4$ ),  $\diamond$  augite ( $CaFeSi_2O_6$ ),  $\bullet$  wollastonite ( $CaSiO_3$ ),  $\blacklozenge$  andradite ( $Ca_3Fe_{2+3}(SiO_4)_3$ ),  $\ast$  vuagnatite ( $CaAlSiO_4(OH)$ ),  $\blacklozenge$  tricalcium aluminate ( $Ca_3Al_2O_6$ ),  $\blacktriangledown$  calcium aluminate oxide ( $Ca_2Al_2O_5$ )].

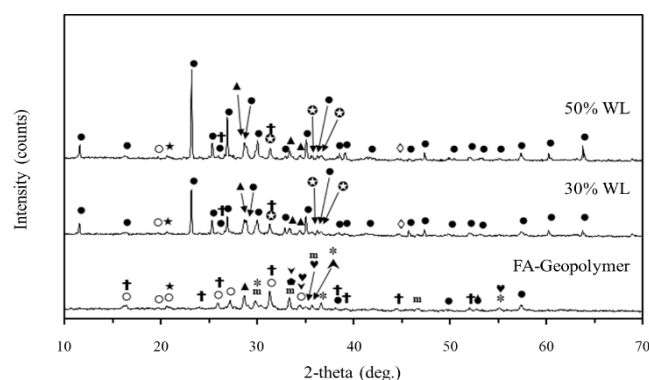


**Figure 15.** XRD patterns of the geopolymer and geopolymer composites reinforced with 30 wt% and 50 wt% wollastonite after firing at 1000°C [ $\dagger$  gehlenite ( $Ca_2Al_2SiO_7$ ),  $\blacktriangle$  kalsilite ( $KAlSiO_4$ ),  $\bullet$  wollastonite ( $CaSiO_3$ ),  $m$  mayenite ( $Ca_{12}Al_{14}O_{33}$ ),  $\star$  quartz ( $SiO_2$ ),  $\blacktriangle$  magnesioferrite ( $MgFe_2O_4$ ),  $\blacklozenge$  andradite ( $Ca_3Fe_{2+3}(SiO_4)_3$ ),  $\ast$  vuagnatite ( $CaAlSiO_4(OH)$ ),  $\circ$  potassium aluminium silicate ( $K_4Al_2Si_2O_9$ ),  $\blacklozenge$  tricalcium aluminate ( $Ca_3Al_2O_6$ ),  $\blacktriangledown$  calcium iron oxide ( $CaFe_4O_7$ ),  $\diamond$  calcium aluminium oxide ( $Ca_3Al_2O_6$ ),  $\odot$  calcium silicate ( $Ca_2SiO_4$ ),  $\blacktriangledown$  calcium aluminate oxide ( $Ca_2Al_2O_5$ )].

## 4. Conclusions

The geopolymer composite synthesized from high calcium fly ash reinforced by wollastonite fiber can improve the thermal stability up to 1100°C. The results revealed that the addition of wollastonite fiber enhanced the thermal stability of the geopolymer by minimizing the thermal expansion by less than 0.5%. The total weight loss was shifted from 25% of the geopolymer to 12% of the geopolymer composite at 1400°C, which was about a 50% decrease in the value. Although the use of wollastonite significantly improved the thermal stability of the fly ash-based geopolymer, it did not adversely affect mechanical strength. The compressive strength was slightly improved, increasing from 33.3 MPa to 38.4 MPa when 40 wt% to 50 wt% wollastonite fiber was added. In contrast, the flexural strength was particularly enhanced; it increased from 2.1 MPa to 6.8 MPa for the same amount of wollastonite fiber as the compressive strength. The relative residual compressive strength after high-temperature exposures was likely to increase with the amount of wollastonite fiber. The presence of wollastonite fiber acted as the micro-crack bridging leading to the enhancement of the relative residual compressive strength after exposure to high temperatures. Moreover, the thermal stability at 1100°C was clearly seen when added wollastonite fiber more than 30 wt%. Therefore, the addition of wollastonite in a geopolymer almost indicated the prospect of using this geopolymer composite for high-temperature applications.

## Acknowledgment

The authors would like to thank the 100<sup>th</sup> Anniversary Chulalongkorn University Fund for Doctoral Scholarship, Center of Excellence on Petrochemical and Materials Technology (PETROMAT), Chulalongkorn University for financial support in term of Doctoral Scholarship and National Metal and Materials Technology Center (MTEC) for the scientific equipment support.

## References

- [1] J. Davidovits, "Geopolymers - Inorganic polymeric new materials," *Journal of Thermal Analysis*, vol. 37, pp. 1633-1656, 1991.
- [2] X. Y. Zhuang, L. Chen, S. Komarneni, C. H. Zhou, D. S. Tong, H. M. Yang, W. H. Yu, and H. Wang, "Fly ash-based geopolymer: Clean production, properties and applications," *Journal of Cleaner Production*, vol. 125, pp. 253-267, 2016.
- [3] E. Kamseu, C. Djangang, P. Veronesi, A. Fernanda, U. C. Melo, V. M. Sglavo, and C. Leonelli, "Transformation of the geopolymer gels to crystalline bonds in cold-setting refractory concretes: Pore evolution, mechanical strength and microstructure," *Materials and Design*, vol. 88, pp. 336-344, 2015.
- [4] D. L. Y. Kong and J. G. Sanjayan, "Damage behavior of geopolymer composites exposed to elevated temperatures," *Cement and Concrete Composites*, vol. 30, pp. 986-991, 2008.
- [5] L. Zuda, J. Drchalová, P. Rovnaník, P. Bayer, Z. Keršner, and R. Černý, "Alkali-activated aluminosilicate composite with heat-resistant lightweight aggregates exposed to high temperatures: Mechanical and water transport properties," *Cement and Concrete Composites*, vol. 32, pp. 157-163, 2010.
- [6] E. Kamseu, A. Rizzuti, C. Leonelli, and D. Perera, "Enhanced thermal stability in K<sub>2</sub>O-metakaolin-based geopolymer concretes by Al<sub>2</sub>O<sub>3</sub> and SiO<sub>2</sub> fillers addition," *Journal of Materials Science*, vol. 45, pp. 1715-1724, 2010.
- [7] V. F. F. Barbosa and K. J. D. MacKenzie, "Thermal behaviour of inorganic geopolymers and composites derived from sodium polysialate," *Materials Research Bulletin*, vol. 38, pp. 319-331, 2003.
- [8] K. Hemra and P. Aungkavattana, "Effect of cordierite addition on compressive strength and thermal stability of metakaolin based geopolymer," *Advanced Powder Technology*, vol. 27, pp. 1021-1026, 2016.
- [9] S. A. Bernal, J. Bejarano, C. Garzón, R. Mejía De Gutiérrez, S. Delvasto, and E. D. Rodríguez, "Performance of refractory aluminosilicate particle/fiber-reinforced geopolymer composites," *Composites Part B: Engineering*, vol. 43, pp. 1919-1928, 2012.
- [10] L. Vickers, W. D. A. Rickard, and A. Van Riessen, "Strategies to control the high temperature shrinkage of fly ash based geopolymers," *Thermochimica Acta*, vol. 580, pp. 20-27, 2014.
- [11] T. Alomayri, "Effect of glass microfibre addition on the mechanical performances of fly ash-based geopolymer composites," *Journal of Asian Ceramic Societies*, vol. 5, pp. 334-340, 2017.
- [12] P. Nuaklong, A. Wongsu, K. Boonserm, C. Ngohpok, P. Jongvivatsakul, V. Sata, P. Sukontasukkul, and P. Chindaprasit, "Enhancement of mechanical properties of fly ash geopolymer containing fine recycled concrete aggregate with micro carbon fiber," *Journal of Building Engineering*, vol. 41, p. 102403, 2021.
- [13] P. Timakul, W. Rattanaprasit, and P. Aungkavattana, "Enhancement of compressive strength and thermal shock resistance of fly ash-based geopolymer composites," *Construction and Building Materials*, vol. 121, pp. 653-658, 2016.
- [14] P. Timakul, W. Rattanaprasit, and P. Aungkavattana, "Improving compressive strength of fly ash-based geopolymer composites by basalt fibers addition," *Ceramics International*, vol. 42, pp. 6288-6295, 2016.
- [15] S. Wattanasiriwech, F. Arif Nurgesang, D. Wattanasiriwech, and P. Timakul, "Characterisation and properties of geopolymer composite part I: Role of mullite reinforcement," *Ceramics International*, vol. 43, pp. 16055-16062, 2017.
- [16] M. Lahoti, K. H. Tan, and E. H. Yang, "A critical review of geopolymer properties for structural fire-resistance applications," *Construction and Building Materials*, vol. 221, pp. 514-526, 2019.
- [17] M. Nawaz, A. Heitor, and M. Sivakumar, "Geopolymers in construction - recent developments," *Construction and Building Materials*, vol. 260, p. 120472, 2020.
- [18] H. Xue, G. Wang, M. Hu, and B. Chen, "Modification of wollastonite by acid treatment and alkali-induced redeposition for use as papermaking filler," *Powder Technology*, vol. 276, pp. 193-199, 2015.
- [19] M. Abdel Wahab, I. Abdel Latif, M. Kohail, and A. Almasry, "The use of Wollastonite to enhance the mechanical properties

- of mortar mixes,” *Construction and Building Materials*, vol. 152, pp. 304-309, 2017.
- [20] S. K. Saxena, M. Kumar, D. S. Chundawat, and N. B. Singh, “Utilization of wollastonite in cement manufacturing,” *Materials Today: Proceedings*, vol. 29, pp. 733-737, 2020.
- [21] F. H. G. Leite, T. F. Almeida, R. T. Faria, and J. N. F. Holanda, “Synthesis and characterization of calcium silicate insulating material using avian eggshell waste,” *Ceramics International*, vol. 43, pp. 4674-4679, 2017.
- [22] N. A. Nair, and V. Sairam, “Research initiatives on the influence of wollastonite in cement-based construction material- A review,” *Journal of Cleaner Production*, vol. 283, p. 124665, 2021.
- [23] R. I. Khan, and W. Ashraf, “Effects of ground wollastonite on cement hydration kinetics and strength development,” *Construction and Building Materials*, vol. 218, pp. 150-161, 2019.
- [24] H. E. Yücel, and S. Özcan, “Strength characteristics and micro-structural properties of cement mortars incorporating synthetic wollastonite produced with a new technique,” *Construction and Building Materials*, vol. 223, pp. 165-176, 2019.
- [25] S. H. Bong, B. Nematollahi, M. Xia, A. Nazari, and J. Sanjayan, “Properties of one-part geopolymer incorporating wollastonite as partial replacement of geopolymer precursor or sand,” *Materials Letters*, vol. 263, p. 127236, 2020.
- [26] E. I. Diaz, E. N. Allouche, and S. Eklund, “Factors affecting the suitability of fly ash as source material for geopolymers,” *Fuel*, vol. 89, pp. 992-996, 2010.
- [27] Z. Su, L. Guo, Z. Zhang, and P. Duan, “Influence of different fibers on properties of thermal insulation composites based on geopolymer blended with glazed hollow bead,” *Construction and Building Materials*, vol. 203, pp. 525-540, 2019.
- [28] Z. He, A. Shen, Z. Lyu, Y. Li, H. Wu, and W. Wang, “Effect of wollastonite microfibers as cement replacement on the properties of cementitious composites: A review,” *Construction and Building Materials*, vol. 261, p. 119920, 2020.
- [29] J. Archez, N. Texier-Mandoki, X. Bourbon, J. F. Caron, and S. Rossignol, “Influence of the wollastonite and glass fibers on geopolymer composites workability and mechanical properties,” *Construction and Building Materials*, vol. 257, p. 119511, 2020.
- [30] N. Ranjbar, and M. Zhang, “Fiber-reinforced geopolymer composites: A review,” *Cement and Concrete Composites*, vol. 107, p. 103498, 2020.
- [31] T. Bakharev, “Geopolymeric materials prepared using Class F fly ash and elevated temperature curing,” *Cement and Concrete Research*, vol. 35, pp. 1224-1232, 2005.
- [32] D. Papias, I. P. Giannopoulou, and T. Perraki, “Effect of synthesis parameters on the mechanical properties of fly ash-based geopolymers,” *Colloids and Surfaces A: Physicochemical and Engineering Aspects*, vol. 301, pp. 246-254, 2007.
- [33] Y. He, X. Zhao, L. Lu, L. J. Struble, and S. Hu, “Effect of C/S ratio on morphology and structure of hydrothermally synthesized calcium silicate hydrate,” *Journal of Wuhan University of Technology, Materials Science Edition*, vol. 26, pp. 770-773, 2011.
- [34] G. M. Canfield, J. Eichler, K. Griffith, and J. D. Hearn, “The role of calcium in blended fly ash geopolymers,” *Journal of Materials Science*, vol. 49, pp. 5922-5933, 2014.
- [35] A. Wongsu, K. Boonserm, C. Waisurasingha, V. Sata, and P. Chindaprasit, “Use of municipal solid waste incinerator (MSWI) bottom ash in high calcium fly ash geopolymer matrix,” *Journal of Cleaner Production*, vol. 148, pp. 49-59, 2017.
- [36] M. Criado, A. Palomo, and A. Fernández-Jiménez, “Alkali activation of fly ashes. Part 1: Effect of curing conditions on the carbonation of the reaction products,” *Fuel*, vol. 84, pp. 2048-2054, 2005.
- [37] L. Reig, M. M. Tashima, M. V. Borrachero, J. Monzó, C. R. Cheeseman, and J. Payá, “Properties and microstructure of alkali-activated red clay brick waste,” *Construction and Building Materials*, vol. 43, pp. 98-106, 2013.
- [38] W. Zhou, C. Yan, P. Duan, Y. Liu, Z. Zhang, X. Qiu, and D. Li, “A comparative study of high- and low- $Al_2O_3$  fly ash based-geopolymers: The role of mix proportion factors and curing temperature,” *Materials and Design*, vol. 95, pp. 63-74, 2016.
- [39] A. A. Siyal, K. A. Azizli, Z. Man, L. Ismail, and M. I. Khan, “Geopolymerization kinetics of fly ash based geopolymers using JMAK model,” *Ceramics International*, vol. 42, pp. 15575-15584, 2016.
- [40] W. Chen, Y. Liang, X. Hou, J. Zhang, H. Ding, S. Sun, and H. Cao, “Mechanical grinding preparation and characterization of  $TiO_2$ -coated wollastonite composite pigments,” *Materials*, vol. 11, p. 593, 2018.
- [41] P. Duxson, A. Fernández-Jiménez, J. L. Provis, G. C. Lukey, A. Palomo, and J. S. J. Van Deventer, “Geopolymer technology: The current state of the art,” *Journal of Materials Science*, vol. 42, pp. 2917-2933, 2007.
- [42] K. Hemra, S. Yamaguchi, T. Kobayashi, P. Aungkavattana, and S. Jiemsirilers, “Compressive strength and setting time modification of class C fly ash-based geopolymer partially replaced with kaolin and metakaolin,” *Key Engineering Materials*, vol. 766, pp. 157-163, 2018.
- [43] S. Kwon, T. Nishiwaki, H. Choi, and H. Mihashi, “Effect of wollastonite microfiber on ultra-high-performance fiber-reinforced cement-based composites based on application of multi-scale fiber-reinforcement system,” *Journal of Advanced Concrete Technology*, vol. 13, pp. 332-344, 2015.
- [44] J. Temuujin, W. Rickard, and A. Van Riessen, “Characterization of various fly ashes for preparation of geopolymers with advanced applications,” *Advanced Powder Technology*, vol. 24, pp. 495-498, 2013.
- [45] S. M. A. El-Gamal, F. S. Hashem, and M. S. Amin, “Thermal resistance of hardened cement pastes containing vermiculite and expanded vermiculite,” *Journal of Thermal Analysis and Calorimetry*, vol. 109, pp. 217-226, 2012.
- [46] M. Lahoti, K. K. Wong, K. H. Tan, and E. H. Yang, “Effect of alkali cation type on strength endurance of fly ash geopolymers subject to high temperature exposure,” *Materials and Design*, vol. 154, pp. 8-19, 2018.
- [47] M. Yu, E. Bernardo, P. Colombo, A. R. Romero, P. Tatarko, V. K. Kannuchamy, M. M. Titirici, E. G. Castle, O. T. Picot, and M. J. Reece, “Preparation and properties of biomorphic potassium-based geopolymer (KGP)-biocarbon (CB) composite,” *Ceramics International*, vol. 44, pp. 12957-12964, 2018.

- [48] G. Roviello, L. Ricciotti, C. Ferone, F. Colangelo, R. Cioffi, and O. Tarallo, "Synthesis and characterization of novel epoxy geopolymer hybrid composites," *Materials*, vol. 6, pp. 3943-3962, 2013.
- [49] S. Donatello, C. Kuenzel, A. Palomo, and A. Fernández-Jiménez, "High temperature resistance of a very high volume fly ash cement paste," *Cement and Concrete Composites*, vol. 45, pp. 234-242, 2014.
- [50] P. Duxson, G. C. Lukey, and J. S. J. van Deventer, "The thermal evolution of metakaolin geopolymers: Part 2 - Phase stability and structural development," *Journal of Non-Crystalline Solids*, vol. 353, pp. 2186-2200, 2007.
- [51] W. M. Kriven, J. L. Bell, and M. Gordon, "Ceramic Transactions," *Ceramic Transactions*, vol. 260, pp. 227-250, 2016.
- [52] E. Tajuelo Rodriguez, K. Garbev, D. Merz, L. Black, and I. G. Richardson, "Thermal stability of C-S-H phases and applicability of Richardson and Groves' and Richardson C-(A)-S-H(I) models to synthetic C-S-H," *Cement and Concrete Research*, vol. 93, pp. 45-56, 2017.
- [53] Q. Zhang, and G. Ye, "Dehydration kinetics of Portland cement paste at high temperature," *Journal of Thermal Analysis and Calorimetry*, vol. 110, pp. 153-158, 2012.